Cellulose (2021) 28:1633–1646
https://doi.org/10.1007/s10570-020-03628-2

ORIGINAL RESEARCH

Hydrophobic development and mechanical properties of cellulose substrates supercritically impregnated with food-grade waxes

Brenda Hutton-Prager · Kolawole Adenekan · Mitchell Sypnewski · Andrew Smith · Mason Meadows · Clarie Calicdan

Received: 18 June 2020 / Accepted: 12 December 2020 / Published online: 6 January 2021

Abstract Supercritical impregnation may be used to impart specific functional properties into porous substrates such as wood, textiles, or paper. In the current study, food-grade beeswax (BW), carnauba wax (CW) and vegetable wax (VW) were impregnated into paper substrates to improve their hydrophobicity and mechanical strength. The contact angle of impregnated and annealed samples was approximately 110–120° when annealed at 140 °C, and 130° when annealed at 160 °C. SEM analyses revealed that dual micro- and nano-scale roughness was generated in impregnated paper substrates that also underwent annealing. FTIR analysis showed evidence of H-bonding between the waxes and cellulose, but this was more dominant with BW/CW compared with VW due to the different chemical structures of the waxes. Annealed samples showed lower intensity FTIR peaks, tentatively confirming a phase transition of the waxes as a result of the annealing. A reduced tan delta signal up to the secondary alpha transition temperature for paper was observed with BW/CW impregnated samples, indicating the formation of additional chemical bonds between cellulose and wax. Compared with untreated paper substrates, the sharp decrease in storage modulus during degradation occurred at temperatures up to 10 °C higher for wax-impregnated papers, and up to 40 °C lower for baseline papers impregnated and annealed without wax. It is believed that the H-bonds between the waxes and cellulose were able to withstand higher temperatures in the degradation region, thus offsetting the effects of sample preparation.

Keywords Food-grade waxes · Supercritical impregnation · Cellulose · Hydrophobicity · Annealing · Dynamic mechanical analysis

B. Hutton-Prager (✉) · K. Adenekan · M. Sypnewski · A. Smith · M. Meadows · C. Calicdan
Chemical Engineering Department, University of Mississippi, 140 Anderson Hall, University, MS 38677, USA
e-mail: bhprager@olemiss.edu

K. Adenekan
e-mail: kadeneka@olemiss.edu

M. Sypnewski
e-mail: mitchsyp21@gmail.com

A. Smith
e-mail: awsmith8@go.olemiss.edu

M. Meadows
e-mail: mmmeadow@go.olemiss.edu

C. Calicdan
e-mail: cmcalicd@go.olemiss.edu

Introduction

Supercritical impregnation (SCI) of waxes into paper substrates for hydrophobic modification is a small but increasingly popular area of investigation, due to the simplicity of the process and its minimal damage to

the environment. The impregnation process often uses supercritical carbon dioxide ($scCO_2$) as the supercritical fluid (SCF), and the solute is first dissolved into this fluid at appropriate process conditions. The solute-laden $scCO_2$ then passes through a substrate and, due to its liquid like densities, gas-like diffusivities, gas-approaching viscosities, high mass transfer, and low surface tension (Song 2006; Quan et al. 2009), fully penetrates the substrate. The solute originally dissolved into the SCF remains within the substrate upon depressurization of the fluid, and coats the matrix or fibers of the porous substrate rather than just the bulk surface. The entire substrate is therefore modified with the particular functionality of the solute, such as water repellency in the case of wax solutes. This SCI process has direct applications in food packaging products where hydrophobic properties of the package, amongst others, are desired.

The use of edible waxes as hydrophobic solutes for food-based applications to replace organic and fluorine-derived compounds is on the rise (Hagenmaier and Baker 1997; Wang et al. 2016, 2018; Saji 2020). The United States Food and Drug Administration and controls (USFDA) regulates the use of coatings in food-based products. Unfortunately, many sizing chemicals that are used in the fabrication of water-repellent packaging materials are not classified as food-compatible (Wang et al. 2016), but are acceptable provided they do not come into contact with the food itself. Several food-grade waxes such as beeswax (BW), carnauba wax (CW) and vegetable wax (VW) are capable of providing hydrophobic modification on substrates, and BW is being considered as an alternative sizing agent for paper and packaged products (Wang et al. 2014; Reshmi et al. 2017). BW is primarily composed of palmitate, palmitoleate and oleate esters (Tulloch 1980; Abdikheibari et al. 2015) and an approximate chemical formula for beeswax is $C_{15}H_{31}COOC_{30}H_{61}$ (Abdikheibari et al. 2015). Its long hydrocarbon chains and internal chain methylene units in its structure render it an excellent hydrophobic modifier (Kameda 2004; Reshmi et al. 2017). CW is commonly used as a fruit coating due to its ability to extend shelf-life (Li et al. 2016), excellent moisture barrier properties, and good compatibility with food (Chick and Hernandez 2002). Its chemical make-up is mainly fatty esters (80–85%), free alcohols (10–15%), acids (3–6%), and hydrocarbons (1–3%) (Puttalingamma 2014). VW is typically obtained by partial or full hydrogenation of vegetable oils (e.g. soybean or palm oil) (Fei and Wang 2017; Mohanan et al. 2020), but frequently needs further chemical modifications to impart suitable functionality to promote useful physical properties (Fei and Wang 2017). Transesterification of hydrogenated soybean oil for example results in a VW mixture containing several different fractions of acylglycerols (glycerides) (Fei and Wang 2017).

Paper substrates are commonly considered for food packaging applications as they cause less damage to the environment, and are often recyclable depending on the coatings or additives introduced (Del Curto et al. 2016). Cellulose, the key material of paper, is frequently used as a modifier or reinforcement to polymers commonly used in plastic films or other similar applications (Lavoratti et al. 2016), but is itself one of the most widely available and studied biopolymers (Roig et al. 2011; Sofla et al. 2016; Ioelovich 2016). The macromolecular glucose chains pack together closely via hydrogen-bonding (H-bonding) between the –OH groups of the glucose units, forming microfibrils (Sofla et al. 2016), which contain crystalline and amorphous regions. Within each individual fibril are cellulose nanocrystal (CNC, crystalline) and cellulose nanofiber (CNF, amorphous), which render cellulose semi-crystalline in structure. The resulting microfibrils are randomly oriented during the drying of an aqueous suspension, but become somewhat aligned in the machine direction (MD) during production (Girardi et al. 2011), leading to an anisotropic material. However at the microscopic level, the cellulose network usually does not display a strong indication of order (He et al. 2016; Wang et al. 2017; Adenekan and Hutton-Prager 2019). Paper is therefore anisotropic in addition to being semi-crystalline within its fibrous structure.

Dynamic Mechanical Analysis (DMA) is ideal for determining various transitions of a polymer/polymeric composite as it deforms under tension and under the influence of temperature, from solid to melt state. The glass transition temperature (T_g) or alpha transition (T_α) is a well-known and measurable temperature at which the material changes from solid to rubbery state (Dunn 1994). This typically occurs prior to the melting temperature of the polymer, T_m (Dunn 1994). Present only in amorphous or semi-crystalline polymers, the T_g denotes the point at which polymeric chains participate in large-scale movement, resulting in decreased storage modulus (E') and strength (Dunn

1994). In semi-crystalline polymers, a secondary alpha-transition may be observed, $T_{\alpha-2}$, representing slippage of crystal portions over each other. Paper disintegrates rather than changes to a rubbery state, but these transitions are still identifiable (Ioelovich 2016). Impregnating waxes into the fibrous network via SCI will create different or additional chemical interactions between the wax and cellulose fiber, affecting (and hopefully improving) the strength properties of the paper.

While the food-grade waxes being considered in this study are suitable environmentally-friendly and food-friendly alternatives to traditional sizing agents, to date, none have been investigated as hydrophobic modifiers on paper substrates *using SCI methods*. The purpose of this investigation is to use SCI with food-grade waxes to prepare hydrophobically modified paper, and subsequently study: a) the resulting hydrophobic development of the modified substrates; b) the interfacial intermolecular interactions between the impregnated waxes and cellulose; c) the mechanical property changes of the modified paper; and d) the effects of annealing treatment on the modified paper with respect to hydrophobicity, intermolecular interactions, and mechanical property improvement. It is expected that the intermolecular interactions between the waxes and substrate, and changes to these interactions as a result of annealing, will be key in explaining both hydrophobic improvements and mechanical property changes. These insights will be useful in further developing such materials for food packaging (and similar) applications.

Materials and methods

Materials

Yellow Beeswax #423 (BW), Yellow Carnauba wax (CW), and Vegetable wax (VW) were supplied by Koster Keunen, with melting points of 62–65 °C, 80–86 °C, and 44–54 °C respectively. Solutions of BW/CW in a 1:1 ratio were prepared at a concentration of 10 g/L in analytical grade n-heptane (99.5%, Sigma Aldrich), used in combined form to compare with other studies (Zhang et al. 2014). VW solutions in n-heptane were prepared at a concentration of 10 g/L. Carbon dioxide (< 50 ppm moisture) was supplied by Airgas USA, LLC, and was used as the carrier fluid to dissolve the wax/heptane solutions. The cellulose substrate used for all experiments was Whatman filter paper no. 1 (Sigma Aldrich).

Methods

Supercritical impregnation of cellulose substrates was conducted at 22 °C and 200 bar using methods and equipment developed in-house, and described elsewhere (Adenekan and Hutton-Prager 2019). It is acknowledged that these conditions are supercritical in pressure but not temperature. Briefly, wax/heptane solution was first dissolved in $scCO_2$ at the process conditions indicated, and then 6 mL was sent to a vessel containing two strips of filter paper (6 mm × 80 mm), where impregnation proceeded for 15 min prior to depressurization.

Annealing of the prepared substrates took place in a 1300 W oven manufactured by Precision Scientific Inc. Division (Winchester, Virginia) for 4 h, at a variety of different temperatures (80, 110, 140 and 165 °C). The heat treatment process began immediately after the cellulose substrates were impregnated.

Sessile drop CA experiments were performed on a Biolin Scientific OneAttension CA analyser, incorporating a single-liquid automatic dispenser, an inbuilt NAVITAR (model 520931), and OneAttension software. The working fluid was deionized water, delivered as 10 µL droplets and at a rate of 1 µL/s. CA measurements were performed on the prepared substrates immediately after impregnation or impregnation/annealing (Day 0), and then 7 days later to assess time dependency of hydrophobic development.

Scanning Electron Microscope (SEM) imaging of treated and untreated substrates was captured with a JSM-7200 FLV FE-SEM instrument. Samples were pre-coated for 4 min with platinum in a Denton Desk V TSC Sputter Coater, to a film thickness of 25 nm. SEM instrument settings included an acceleration voltage of 5.0 kV, a working distance of 20 mm, and different magnifications (×25–×5000).

Fourier Transform Infra Red (FTIR) measurements were conducted using a Cary 630 (Agilent Technologies) instrument, to identify changes in bonding behavior of the impregnated waxes under different conditions as well as their interactions with the cellulose substrates. The Attenuated Total Reflectance (ATR) mode was used, and transmittance data was

analyzed to identify critical peaks relating to VW, BW/CW, and cellulose.

Thermal and mechanical properties of both treated and untreated substrates were determined using a Q800 Dynamic Mechanical Analyzer, DMA (TA Instruments, DE, USA). A frequency of 1 Hz was used at a temperature range of approximately 40–400 °C, with a heating rate of 5 °C/min. The film tension mode was used, together with OscAmp 15, StaticF 0.01, and ForceTrack 125.0%. The dimensions of the samples were 18 mm long, 6 mm wide and 0.15–0.30 mm thick after cutting the specimens. The thickness was predetermined from Whatman paper, but the length and width dimensions had an error of ± 1 mm. DMA testing was conducted 1–2 days after preparation of plain paper, impregnated paper, and impregnated/annealed paper substrates.

Results and discussion

Hydrophobic development of wax-impregnated papers at different annealing temperatures

Contact angle (CA) analysis

VW and BW/CW mixtures were supercritically impregnated into paper, and annealed at different temperatures, with the hydrophobicity subsequently being assessed by taking contact angle (CA) measurements. In an earlier study by Zhang et al. (2014), a 1:1 mixture of BW/CW was found to provide a wide range of melting temperatures between approximately 45–80 °C. This mixture ratio was maintained in the current study to exploit the melting temperature range during annealing and promote polymorphic phase separation (Zhang et al. 2014). During phase separation, wax components from an impure mixture separate out and re-form with a new surface morphology and roughness profile, thereby improving the hydrophobicity (Zhang et al. 2014).

CA vs time plots are shown in Fig. 1 for both wax mixtures (VW and BW/CW). The error in CA values from countless experiments conducted both here and in earlier work (Adenekan and Hutton-Prager 2019) is typically no more than ± 5° (1 standard deviation). VW data in Fig. 1a shows very little hydrophobic development with annealing temperatures of 105 °C, but was considerable at 140 and 160 °C. These results were repeated one week later, and results are similar, with those at 140 °C being just outside the experimental error margin. In this case, there is a small worsening of the surface hydrophobicity.

BW/CW data in Fig. 1b taken on Day 0 shows little hydrophobic development at the 80 °C annealing temperature, but moderate development at 110 °C, in contrast to the VW studies which showed little development at a similar temperature of 105 °C. However, both sets of studies show that considerable hydrophobicity was achieved with annealing temperatures at 140 °C and higher, and subsequently, an annealing temperature of 140 °C was chosen for most DMA studies. It is important to note that additional studies with these same waxes and with no annealing treatment showed very little development in hydrophobicity on Day 0, with low values of CA recorded at short times, as reported elsewhere (Adenekan 2019). This confirms that the annealing temperature is important, and the applied heat energy is responsible for altering surface morphology of the impregnated samples as a result of polymorphic phase separation.

The BW/CW data in Fig. 1b at first appears contradictory to earlier studies performed with BW/CW applied coatings to paper substrates by Zhang et al. (Zhang et al. 2014), where they reported superhydrophobic surfaces for all prepared samples (12 h annealing between 25 and 80 °C). However, in their work, they used A4 copy paper, which is typically already sized (Iselau et al. 2018), while for the surface coating they used molten BW/CW along with cetyltrimethyl ammonium bromide (CTAB), a known hydrophobic modifier, and latex. Removing the several 'hydrophobic helpers' within their study, and considering only the hydrophobic effects of the waxes, shows that significantly higher annealing temperatures are required to achieve hydrophobic (not superhydrophobic) conditions. In another study of wood samples impregnated with beeswax via a dipping wax bath at 120 °C (3 or 6 h) (Li et al. 2020), typical CA were no more than approximately 128°, more in keeping with the present results.

SEM images in Fig. 2 compare the changes in physical structure of the impregnated paper substrates before and after annealing at 140 °C for 4 h. The lower magnification images (Fig. 2a–d) show a more even distribution of VW through the matrix after annealing, while both show a more porous structure.

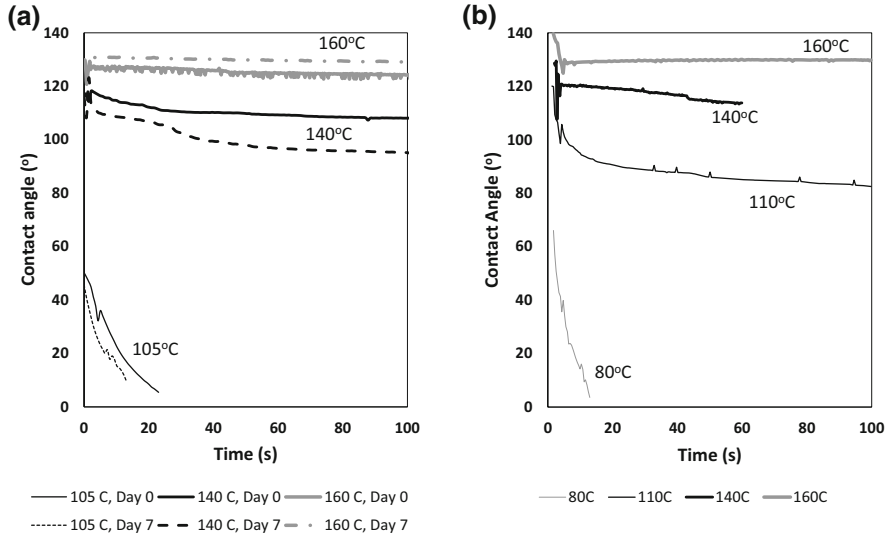

Fig. 1 CA measurements on paper substrates impregnated at 200 bar, 20 °C with **a** VW tested Day 0 and Day 7; and **b** BW/CW tested Day 0, annealed at different temperatures for 4 h duration

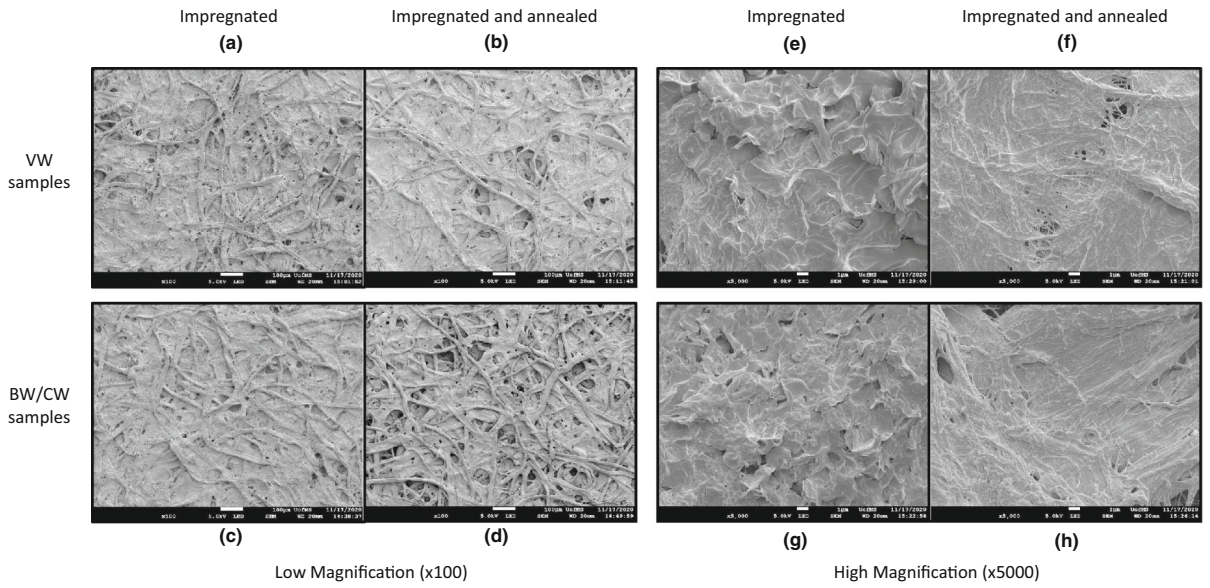

Fig. 2 SEM images of wax-impregnated papers (10 g/L, 200 bar, 20 °C), before and after annealing (4 h, 140 °C). Low magnification images of **a** VW impregnated; **b** VW impregnated + annealed; **c** BW/CW impregnated; and **d** BW/CW impregnated and annealed, showing repositioning of the waxes as a result of annealing treatment. High magnification images **e**–**h** of the same conditions, respectively, showing the structural changes resulting from annealing that contributed to a higher CA

Higher porosity surfaces tend to favor a higher CA, as per Cassie-Baxter theory (Rutter and Hutton-Prager 2018). The higher magnification images (Fig. 2e–h) show a substantial change in morphology of the annealed samples for both wax samples considered. Before annealing, relatively large wave-like and flake-like deposits of VW and BW/CW are observed, up to approximately 5 μm in diameter for VW and 2–3 μm for BW/CW. After annealing, a small quantity of similar-shaped deposits remain at sub-micron size ($\sim$ 0.5 to 1 μm), but the predominant surface is now a more continuous, very fine, stringy and fibrous-type structure at approximately 100 nm diameter. The generation of dual-scale, micro-/nano- roughness on

the surface greatly contributed to the enhanced hydrophobicity of the annealed samples, a phenomenon that is similarly used to confirm hydrophobic improvements by several others studying different systems (Zhang et al. 2017; Chen et al. 2018; Adenekan and Hutton-Prager 2019).

Solute chemical structure, and bonding between solute and substrate

The chemical make-up of the impregnated molecules is also an important consideration contributing to hydrophobicity, both in terms of its actual hydrophobic content and its interactions with the cellulose molecules. Polymorphic phase transitions in beeswax, for example, showed four different transitions during heating, some of which were associated with transitions from orthorhombic to rotator phase structure, and from trans $–CH_2–$ chains to gauche-trans conformations (Gaillard et al. 2011). These transitions, apart from generating physical structural changes, may also contribute to improved bonding between wax and substrate once the annealing treatment is completed. All three food-grade waxes have similar ester functional groups, but are arranged differently. In BW and CW, the single esters are likely to be within a single hydrocarbon chain, and are less hindered to participate in H-bonding with the –OH groups on cellulose fibers. VW also has ester groups, but these are typically present within glycerides, and such a backbone may somewhat restrict the freedom of these groups to participate to the same extent in a similar H-bonding process. Figure 3 shows generic chemical structures of some typical functional groups likely to be present in these waxes.

The annealing temperatures used rendered each wax in liquid form, with the vaporization points at least 100 °C higher for BW/CW (Galvão et al. 2020) and the melting points approximately 60–90 °C lower, depending on the wax. After the heating process was completed and the impregnated samples returned to room temperature, the structural changes occurring as a result of the heat treatment may have enabled the ester functional groups to better align with the –OH groups on the cellulose to create additional H-bonds. If it is assumed that, in this arrangement, the hydrocarbon chains are pointing away from the cellulose, this represents a plausible chemical explanation of why a better surface was achieved with BW/CW impregnations compared with VW at similar temperatures. The applied heat energy (and subsequent solidification) certainly allowed the solid wax particles to melt and redistribute as a more continuous film, in better contact with the cellulose fibers (see Fig. 2).

This theory is also tentatively supported when considering the FTIR spectra of VW and BW/CW modified substrates (Fig. 4), all normalized by subtracting the plain paper trace from the absorbance values. As previously mentioned, all waxes have similar chemical content, but it is their interaction with cellulose that will provide added information into the likely orientations of these molecules. Also of note with the FTIR traces are the changes, particularly in peak height, with annealing treatment. One of the most important peaks in all traces is the low, broad peak occurring approximately at 3325 cm^{-1}. Since the input from cellulose has been subtracted from these

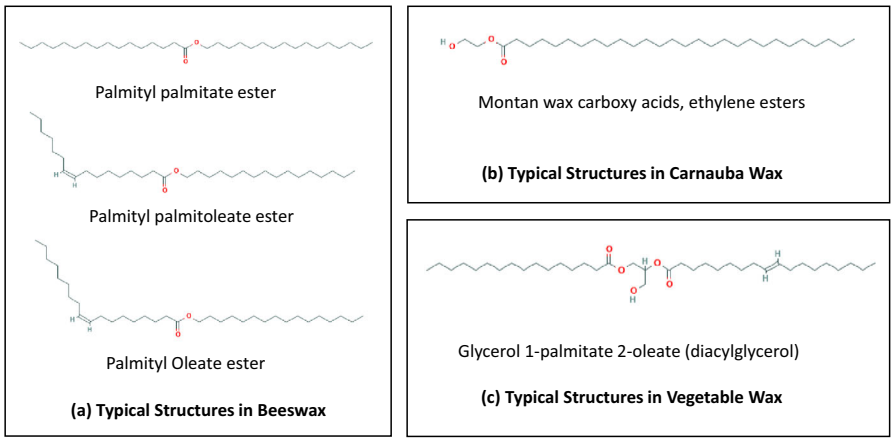

Fig. 3 Examples of chemical structures likely to be present within **a** Beeswax (National Center for Biotechnology Information 2020a, b, c); **b** Carnauba wax (National Center for Biotechnology Information 2020d); and **c** vegetable wax (National Center for Biotechnology Information 2020e)

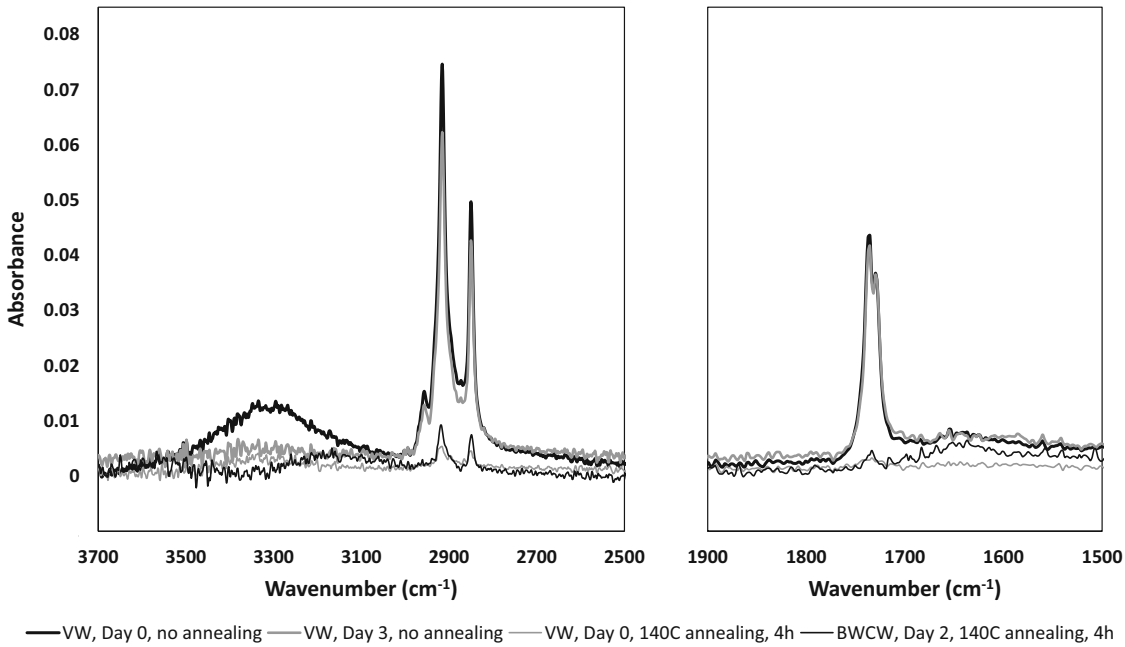

Fig. 4 FTIR traces of paper samples impregnated with VW or BWCW, and assessed immediately after preparation (Day 0), Day 2, and Day 3. Some samples were prepared with 4 h annealing, at 140 °C

traces, any remaining peak is due to additional –OH groups from the waxes. Fatty acids and free alcohols are frequently present in these waxes, as confirmed by this peak. For VW, this peak reduces from Day 0 to day 3 potentially due to natural losses, but reduces further upon the addition of heat (the annealing treatment), likely causing some evaporation of these alcohol groups or other impurities within the waxes (Buchwald et al. 2008). The peak position remains approximately constant for all the VW traces. For the BW/CW trace, this peak is also low due to the annealing treatment, but is distinctly red-shifted from those observed with the VW traces, a phenomenon often observed when there is significant H-bonding (Gonjo et al. 2011). The shift moved from approximately 3325 to 3150 cm^{-1}, and is a good indicator of the likelihood of more abundant H-bonding with this wax mixture compared with the VW.

Besides the broad peak at 3325 cm^{-1}, the non-annealed VW-treated substrates over different days show several peaks relating to C-H, $–CH_2$ or $–CH_3$ bending and stretching vibrations (2960 cm^{-1}: stretching from $–CH_3$, $–CH_2$ and –CH (McMurry 2012); 2915–2920 cm^{-1}: C–H stretching (Shen et al. 2005) or additional contributions to the –OH broad peak (Nibbering et al. 2007); 2850 cm^{-1}: additional C–H stretching (Shen et al. 2005); 1475 cm^{-1}: $–CH_2$ bending (Shen et al. 2005)). Two additional peaks related to functional groups present in VW were observed at 1740 cm^{-1} (–C=O stretching) and 1650 cm^{-1} (C=C stretching) (McMurry 2012). Comparing these peak profiles with the annealed VW-treated substrate, the peak height had drastically reduced in all cases, and peaks at 2960, 1740, and 1650 cm^{-1} had disappeared. Overall reduction in peak intensity may indicate a change in phase transition of the sample components as a result of annealing (less intensity of the stretching and bending vibrations) (Mallamace et al. 2015; Nivitha et al. 2019). The disappearance of the 1740 and 1650 cm^{-1} tends to align well with the polymorphic phase separation and regrouping of wax components upon heating, which may account for a reduction in the prominence of these functional groups.

Only the annealed sample for BW/CW was considered for FTIR analysis, and given the similarities of chemical content with VW, similar peak-positions were noted. Also noted were similar reduced-

amplitude peaks for this annealed sample. However, the BW/CW showed a stronger peak (even though annealed) at 1650 cm^{-1} (C=C stretching), likely indicative of different molecular make-up of the wax and potentially different rearrangements of the wax components during polymorphic phase separation.

The FTIR traces demonstrate the drastic structural changes caused by the annealing process and also the more abundant H-bonding of the BW/CW to the paper substrates, contributing to a more hydrophobic surface.

Mechanical properties of wax-impregnated and annealed papers

The preceding section has established that the introduction of food-grade waxes into paper substrates via SCI methods and annealing treatments has allowed the development of a hydrophobic surface, together with additional H-bonding between the waxes and substrate. This section investigates the strengthening effects of the wax solutes into the paper substrates.

Mechanical analysis of plain paper

The mechanical properties of the paper substrate prior to impregnation and/or heat treatment were determined to establish a baseline from which changes may be compared. DMA analysis of three plain paper samples were investigated: untreated plain paper; plain paper impregnated with $scCO_2$/heptane (no wax); and plain paper impregnated with $scCO_2$/heptane (no wax) and 4 h annealing conducted at 140 °C. The latter two samples were tested 1–2 days after treatment.

Storage (E′) and loss (E″) moduli, together with the corresponding tan delta information for these three samples are shown in Fig. 5a, where tan delta is the ratio of loss to storage moduli. The storage moduli each follow a similar shape until approximately 250 °C, although the moduli decrease in the order of plain paper, CO_2/n-heptane impregnated paper, and impregnated-annealed paper (RSD for plain paper is 0.15). The storage modulus is an indicator of stored or elastic energy within a material, and the effects of SCI and annealing treatments appear to reduce the stiffness of the plain paper sample somewhat, even at lower temperatures. Above 250 °C, while E′ continues to gently decrease for the plain paper sample, it starts a more rapid descent for the other two treated samples, denoting a stronger reduction in elastic properties. A similar behavior is also observed with the loss moduli curves at these higher temperatures, where the treated paper samples demonstrate a reduction in energy or viscous dissipation. Scission of molecules is believed to occur when both storage and loss moduli reduce (Willoughby 2016), which is in keeping with these temperatures as they approach the degradation temperature of paper.

Whatman paper begins to degrade at approximately 275 °C confirmed elsewhere by differential scanning calorimetry (DSC) (Soares et al. 1995), and a small rise in the tan delta signal is observed between 270 and 290° across all samples tested. The onset of the main tan delta peak at approximately 320 °C, also corresponding to a significant drop in the E′ of plain paper, is thought to be linked to the maximum rate of weight loss of the sample, determined by DSC studies to be between 331 and 332 °C (Soares et al. 1995). Physical inspection of the samples at this point confirmed the loss of mass. The major tan delta peak occurred at approximately 340 °C for all paper samples, and is likened to an endotherm recorded at 340–343 °C by DSC (Soares et al. 1995). This endotherm is the point at which cellulose undergoes depolymerization, however, was not confirmed with FTIR (or other) measurements in the present study.

The T_g of paper was reported as 217–227 °C (Ioelovich 2016), and a gentle peak in the tan delta curves is observed around this temperature. The T_g particularly can be largely influenced by factors such as the effects of MD vs cross-machine direction (CD) during paper manufacture (Girardi et al. 2011); moisture variations (Ioelovich 2016); the degree of crystallinity of the paper (Ioelovich 2016); and prior thermal history of the samples (Wada et al. 2003). In a study by Wada, Kondo and Okano (Wada et al. 2003), X-ray diffraction measurements showed a hysteresis in heating and cooling of cellulose between room temperature and 300 °C, at a heating rate of 5 °C/min. FTIR studies also showed small changes in peaks after a heat treatment performed at 300 °C for 5 min. These changes were attributed to different crystalline structures of cellulose brought on by the applied heat, which was partially explained by a rearrangement of H-bonds within the samples. It is possible therefore, that similar changes or rearrangements in H-bonding occurred in the paper sample during the annealing

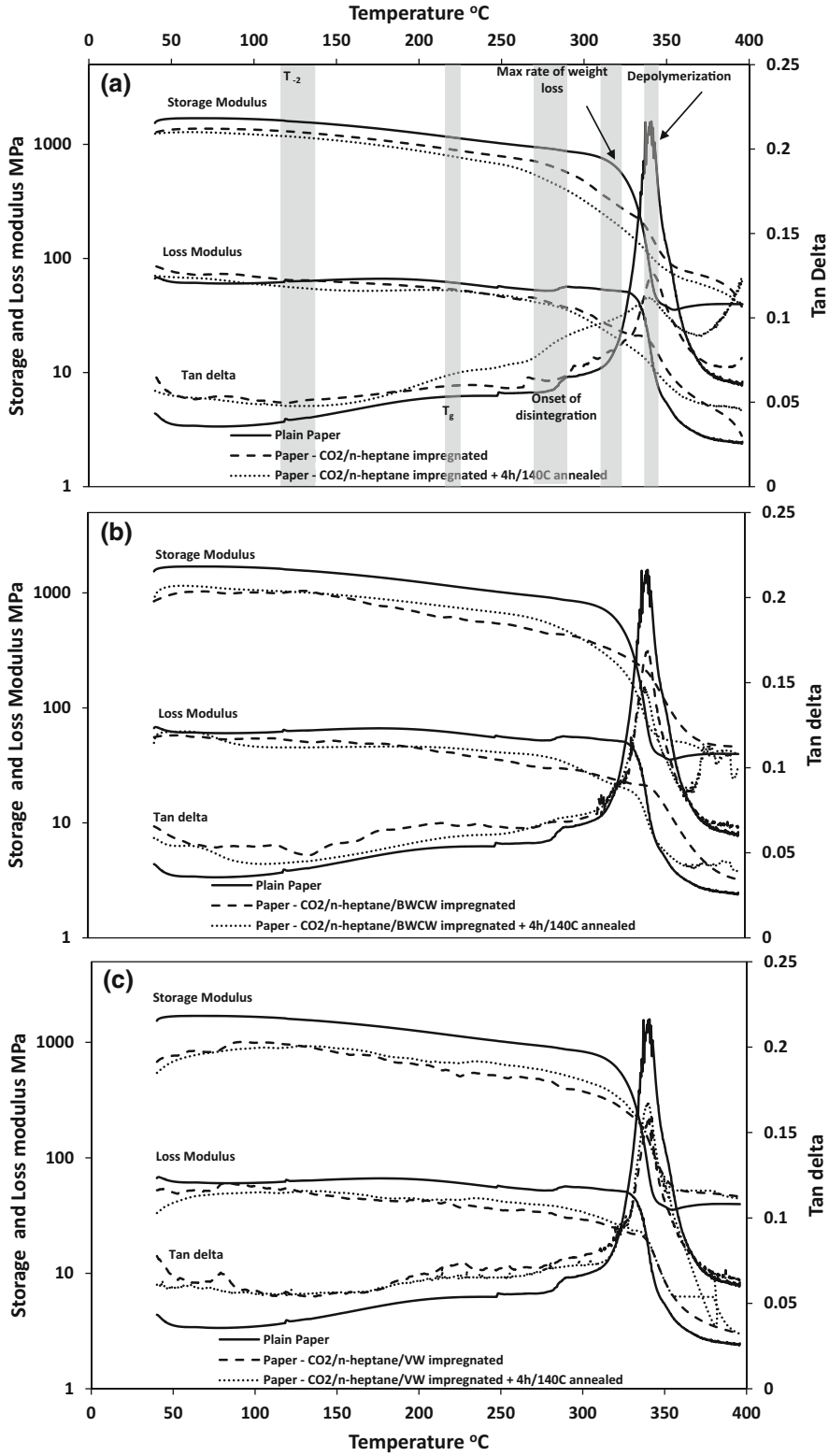

Fig. 5 Storage modulus, loss modulus, and tan delta information for **a** Plain paper with impregnation and annealing treatments; **b** paper treated with BW/CW; and **c** paper treated with VW. Untreated plain paper data has been plotted on all graphs for comparison with the wax-impregnated papers. The greyed regions in **a** indicate where the $T_{\alpha-2}$, T_g, onset of disintegration, maximum rate of weight loss, and depolymerization of cellulose occur

treatment, subsequently affecting the mechanical properties of the paper. The $T_{\alpha-2}$ coincided with the first drop in E′, measured for plain paper at 118 °C, representing movement of the crystalline portions over each other (Dunn 1994).

Mechanical analysis of wax-impregnated papers

DMA data was similarly obtained for paper substrates impregnated with BW/CW and VW, and is shown in Fig. 5b, c respectively, together with the plain paper data replotted for comparison. The impregnated and impregnated-annealed samples for both waxes again showed a slightly lower storage and loss modulus compared with untreated plain paper, and similar key features identified with the tan delta plots were still present. However, comparing the storage moduli of wax-impregnated and impregnated-annealed samples with their respective treated plain paper samples revealed that the overall stiffness of all samples was approximately within one standard deviation error. This result explicitly demonstrates that the introduction of the wax components does not further reduce the overall stiffness of the paper. The temperature at maximum rate of weight loss of the samples was 10 °C higher than that observed with plain paper (see Table 1), and up to 50 °C higher than that recorded for treated plain paper samples. This is significant, because it suggests that not only does the presence of impregnated wax extend the temperature range prior to degradation, it also offsets the effects of SCI and annealing treatments. The additional H-bonding between wax molecules and cellulose is instrumental in enabling the composite material to withstand higher temperatures.

The BW/CW impregnated and annealed samples in particular showed a small but steady decrease in tan delta value up to the $T_{\alpha-2}$ region, before following the upward trend of the plain paper trial from thereon in. The melting point range for a BW/CW 1:1 composition is 45–80 °C (Buchwald et al. 2008; Zhang et al. 2014)). This range begins lower than the individual melting points of the waxes, in keeping with standard solid–liquid phase diagrams, but also dependent upon the eutectic point of the mixture (Yuan et al. 2016). As the temperature is increased in this region, the opportunity for H-bonding between the ester groups in the wax samples and the –OH groups of the cellulose improves (refer again to Fig. 3 for typical wax molecular structures) due to better contact between a liquid-forming wax and the substrate. The overall increase in bonds is associated with a strengthened material, and the small decrease in tan delta value observed (E′ increasing and/or E″ decreasing) may offer some support for this theory. These trends were also observed in the creation of crosslinks during the vulcanization of rubbers (Willoughby 2016). Similar behavior is likely to have occurred with the VW samples as well, but with greater difficulty in creating H-bonds as observed with FTIR data (Fig. 4) and the chemical structure of these waxes (Fig. 3), this was more difficult to confirm with the DMA studies.

As the temperature continued to increase through the $T_{\alpha-2}$ region (117–137 °C) (Ioelovich 2016), both the now fully liquid waxes and the paper substrate itself were contributing to an increase in E″.

Table 1 Point of maximum rate of weight loss of plain paper and treated papers

Sample description	Annealing conditions	Temperature at maximum rate of weight loss (°C)
Plain filter paper	None	320
Paper/CO_2/n-heptane	None	285
	4 h, 140 °C	275
VW/CO_2/n-heptane	None	330
	4 h, 140 °C	328
BW/CW/CO_2/n-heptane	None	330
	4 h, 140 °C	320

Temperatures were determined graphically from the intersection of the two tangents on the E′ curve at the point of rapid E′ reduction

The role of molecular interactions in complex, modified substrates

Some brief comments are warranted to round off this discussion, and highlight the importance and wide-reaching effects of molecular interactions on the macro-physical properties of composite materials.

This investigation began by preparing cellulose substrates using the relatively unique SCI method to uniformly impart hydrophobic waxes onto the fiber surfaces. FTIR studies confirmed that H-bonding between the waxes and cellulose substrates was likely, and annealing the samples (typically for 4 h, 140 °C) tended to alter the chemical bonding of the wax as well as between the wax and substrate. The much-reduced vibrational peaks tentatively confirmed phase transitions of the wax components that resulted with the annealed samples, and SEM images also revealed a drastically altered morphology.

CA analysis revealed that hydrophobicity of the cellulose substrates was greatly improved from plain paper values, and that a higher annealing temperature resulted in a higher CA. Interpretations of DMA measurements showed that the presence of the wax solutes in the substrates did not detract from the overall stiffness of the materials, and may have indicated a slight improvement in stiffness at lower temperatures for the BW/CW impregnated papers (decrease in tan delta value). Wax-treated papers withstood the effects of higher temperatures due to the enhanced H-bonding (higher temperatures observed at maximum rate of weight loss). SCI is a very efficient method to uniformly introduce solute throughout an entire substrate, leading to enhanced opportunity for intermolecular interactions.

By carefully controlling, and in fact influencing, these intermolecular interactions, one can positively affect several physical properties, in this case, improved hydrophobicity and at least maintenance of mechanical strength. While hydrophobicity and mechanical strength of a modified substrate are not directly related, they both depend on similar molecular-level interactions for their optimization. Both these properties are highly important in the design and development of innovative food packaging, and it is clear that the properties at the interfacial molecular level have a direct impact on the bulk properties of a composite material.

Conclusions

Paper substrates were supercritically impregnated with food-grade waxes to investigate improvement to their hydrophobicity and mechanical properties, for potential use in packaging applications. Subsequent analysis of these samples revealed novel information about these uniquely treated papers from both a chemical and mechanical viewpoint. CA measurements of prepared samples showed that a 4 h annealing treatment of at least 140 °C was required to create a sufficiently hydrophobic surface between 110 and 120°, while 160 °C annealing temperatures rendered a hydrophobic surface of approximately 130°. SEM micrographs showed the development of a dual micro-/nano-scale surface with annealed samples, commonly known to greatly contribute to hydrophobicity. The annealing process also tended to distribute the waxes over the cellulose fibers as a somewhat continuous thin film, compared with more solid, discrete wax particles resulting from the impregnation process. Corresponding FTIR traces revealed stronger H-bonding between BW/CW and cellulose compared with VW and cellulose, likely due to less hindered functional groups. Lower intensity peaks observed with annealed samples suggest polymorphic phase separation of the waxes during annealing.

DMA analysis of the impregnated and impregnated/annealed papers also tentatively confirmed the creation of H-bonding between the waxes and cellulose, particularly for BW/CW samples, where the tan delta signal reduced with temperature up to approximately 120 °C. The temperature at which E′ decreased rapidly, corresponding to the rate of maximum weight loss of the sample, was recorded at 320 °C for plain paper samples, and is well correlated with other researchers. Impregnation and impregnation/annealing treatments reduced this temperature by 40 °C, however the intermolecular interactions between impregnated waxes and cellulose not only made up this shortfall but also extended this temperature by an additional 10 °C. Therefore, there was a greater ability of these samples to withstand higher temperatures in the degradation temperature region of paper, and overcome the reduction in storage modulus as a result of SCI and annealing treatments.

Such results are believed to be the first reported in the literature for these SCI systems, and are critical in the development of composite materials for functional

packaging applications. The intermolecular interactions between waxes and cellulose were found duly responsible for modifying the overall mechanical properties and hydrophobicity of the substrates.

Acknowledgments This work has been funded by internal resources at the University of Mississippi. Scanning Electron Microscopy images presented in this work were generated using the instruments and services at the Microscopy and Imaging Center, The University of Mississippi. This facility is supported in part by Grant 1726880, National Science Foundation.

Authors' contributions All authors contributed to the study conception and design. Material preparation and data collection were performed by Kolawole Adenekan, Mitchell Sypnewski, Andrew Smith, Mason Meadows and Clarie Calicdan. Brenda Prager and Kolawole Adenekan performed analysis, and co-wrote the first draft. All subsequent drafts, analysis, and final manuscript were written by Brenda Prager. All authors read and approved the final manuscript.

Availability of data and material All experimental data will be made available upon request to the corresponding author.

Compliance with ethical standards

Conflict of interest The authors declare that they have no conflict of interest.

Consent for publication All authors provided email consent agreeing to the publication upon receiving the final draft for consideration.

Ethics approval This article does not contain any studies with human participants or animals performed by any of the authors.

References

Abdikheibari S, Parvizi R, Moayed M et al (2015) Beeswax-colophony blend: a novel green organic coating for protection of steel drinking water storage tanks. Metals 5:1645–1664. https://doi.org/10.3390/met5031645

Adenekan K (2019) Hydrophobization of cellulose-based fibers for packaging applications with alkyl ketene dimers (AKD) and food-grade waxes via supercritical impregnation with carbon dioxide: experimental and thermodynamic modeling approaches. Ph.D. dissertation, University of Mississippi

Adenekan K, Hutton-Prager B (2019) Sticky hydrophobic behavior of cellulose substrates impregnated with alkyl ketene dimer (AKD) via sub- and supercritical carbon dioxide. Colloids Surf Physicochem Eng Asp 560:154–163. https://doi.org/10.1016/j.colsurfa.2018.09.073

Buchwald R, Breed MD, Greenberg AR (2008) The thermal properties of beeswaxes: unexpected findings. J Exp Biol 211:121–127. https://doi.org/10.1242/jeb.007583

Chen S, Song Y, Xu F (2018) Highly transparent and hazy cellulose nanopaper simultaneously with a self-cleaning superhydrophobic surface. ACS Sustain Chem Eng 6:5173–5181. https://doi.org/10.1021/acssuschemeng.7b04814

Chick J, Hernandez RJ (2002) Physical, thermal, and barrier characterization of casein-wax-based edible films. J Food Sci 67:1073–1079. https://doi.org/10.1111/j.1365-2621.2002.tb09455.x

Del Curto B, Barelli N, Profaizer M et al (2016) Poly-paper: a sustainable material for packaging, based on recycled paper and recyclable with paper. J Appl Biomater Funct Mater. https://doi.org/10.5301/jabfm.5000335

Dunn AS (1994) Introduction to physical polymer science (2nd edition). By L. H. Sperling, New York, 1992 John Wiley & Sons Inc. John Wiley & Sons Inc., New York, 1992. pp. xxvii + 594, price £55.00. ISBN 0-471-53035-2. Polym Int 33:233–233. https://doi.org/10.1002/pi.1994.210330214

Fei T, Wang T (2017) A review of recent development of sustainable waxes derived from vegetable oils. Curr Opin Food Sci 16:7–14. https://doi.org/10.1016/j.cofs.2017.06.006

Gaillard Y, Mija A, Burr A et al (2011) Green material composites from renewable resources: Polymorphic transitions and phase diagram of beeswax/rosin resin. Thermochim Acta 521:90–97. https://doi.org/10.1016/j.tca.2011.04.010

Galvão JG, Santos RL, Lira AAM et al (2020) Stearic acid, beeswax and carnauba wax as green raw materials for the loading of carvacrol into nanostructured lipid carriers. Appl Sci 10:6267. https://doi.org/10.3390/app10186267

Girardi F, Maggini S, Della Volpe C et al (2011) Hybrid organic–inorganic materials on paper: surface and thermomechanical properties. J Sol-Gel Sci Technol 60:315–323. https://doi.org/10.1007/s10971-011-2563-z

Gonjo T, Futami Y, Morisawa Y et al (2011) Hydrogen bonding effects on the wavenumbers and absorption intensities of the oh fundamental and the first, second, and third overtones of phenol and 2,6-dihalogenated phenols studied by visible/near-infrared/infrared spectroscopy. J Phys Chem A 115:9845–9853. https://doi.org/10.1021/jp201733n

Hagenmaier RD, Baker RA (1997) Edible coatings from morpholine-free wax microemulsions. J Agric Food Chem 45:349–352. https://doi.org/10.1021/jf9604551

He M, Cho B-U, Won JM (2016) Effect of precipitated calcium carbonate—Cellulose nanofibrils composite filler on paper properties. Carbohydr Polym 136:820–825. https://doi.org/10.1016/j.carbpol.2015.09.069

Ioelovich M (2016) Isophase transitions of cellulose: a short review. Athens J Sci 3:309–322. https://doi.org/10.30958/ajs.3-4-4

Iselau F, Malmborg-Nystrm K, Holmberg K, Bordes R (2018) Parameters influencing hydrophobization of paper by surface sizing. Nord Pulp Pap Res J 33:95–104. https://doi.org/10.1515/npprj-2018-3015

Kameda T (2004) Molecular structure of crude beeswax studied by solid-state 13C NMR. J Insect Sci. https://doi.org/10.1093/jis/4.1.29

Lavoratti A, Scienza LC, Zattera AJ (2016) Dynamic-mechanical and thermomechanical properties of cellulose nanofiber/polyester resin composites. Carbohydr Polym

136:955–963. https://doi.org/10.1016/j.carbpol.2015.10.008

Li P, Li H, Yang J, Meng Y (2016) Facile fabrication of superhydrophobic paper with excellent water repellency and moisture resistance by phase separation. BioResources 11:6552–6565

Li Y, Qian J, Wang Z et al (2020) Effect of beeswax impregnation on the dimensional stability, surface properties, and thermal characteristics of wood. BioResources 15:2181–2194

Mallamace F, Corsaro C, Mallamace D et al (2015) Water and lysozyme: some results from the bending and stretching vibrational modes. Front Phys. https://doi.org/10.1007/s11467-015-0488-7

McMurry J (2012) Organic chemistry. Brooks/Cole Cengage Learning, Singapore

Mohanan A, Bouzidi L, Narine SS (2020) Waxes derived from self-metathesis modified plant oil blends: A case for exploiting oligomerization to mitigate low molecular mass and unsaturation. Ind Crops Prod 143:111936. https://doi.org/10.1016/j.indcrop.2019.111936

National Center for Biotechnology Information (2020a) PubChem compound summary for CID 10889, cetyl palmitate. https://pubchem.ncbi.nlm.nih.gov/compound/Cetyl-palmitate. Accessed 27 Nov 2020

National Center for Biotechnology Information (2020b) PubChem compound summary for CID 5363258, palmityl palmitoleate. https://pubchem.ncbi.nlm.nih.gov/compound/Palmityl-palmitoleate. Accessed 27 Nov 2020

National Center for Biotechnology Information (2020c) PubChem compound summary for CID 5377655, palmityl oleate. https://pubchem.ncbi.nlm.nih.gov/compound/Palmityl-oleate. Accessed 27 Nov 2020

National Center for Biotechnology Information (2020d) PubChem summary for CID 3018404, fatty acids, montan-wax, ethylene esters. https://pubchem.ncbi.nlm.nih.gov/compound/Fatty-acids_-montan-wax_-ethylene-esters. Accessed 27 Nov 2020

National Center for Biotechnology Information (2020e) PubChem compound summary for CID 6026790, diacylglycerol. https://pubchem.ncbi.nlm.nih.gov/compound/Diacylglycerol. Accessed 27 Nov 2020

Nibbering ETJ, Dreyer J, Kühn O et al (2007) Vibrational dynamics of hydrogen bonds. In: Kühn O, Wöste L (eds) Analysis and control of ultrafast photoinduced reactions. Springer, Berlin, pp 619–687

Nivitha MR, Prasad E, Krishnan JM (2019) Transitions in unmodified and modified bitumen using FTIR spectroscopy. Mater Struct. https://doi.org/10.1617/s11527-018-1308-7

Puttalingamma V (2014) Edible coatings of carnauba wax – a novel method for preservation and extending longevity of fruits and vegetables - a review. Internet J Food Saf 16:1–5

Quan C, Werner O, Wagberg L, Turner C (2009) Generation of superhydrophobic paper surfaces by a rapidly expanding supercritical carbon dioxide? Alkyl ketene dimer solution. J Supercrit Fluids 49:117–124. https://doi.org/10.1016/j.supflu.2008.11.015

Reshmi CR, Sundaran SP, Juraij A, Athiyanathil S (2017) Fabrication of superhydrophobic polycaprolactone/beeswax electrospun membranes for high-efficiency oil/water separation. RSC Adv 7:2092–2102. https://doi.org/10.1039/C6RA26123J

Roig F, Dantras E, Dandurand J, Lacabanne C (2011) Influence of hydrogen bonds on glass transition and dielectric relaxations of cellulose. J Phys Appl Phys 44:045403. https://doi.org/10.1088/0022-3727/44/4/045403

Rutter T, Hutton-Prager B (2018) Investigation of hydrophobic coatings on cellulose-fiber substrates with in situ polymerization of silane/siloxane mixtures. Int J Adhes Adhes 86:13–21. https://doi.org/10.1016/j.ijadhadh.2018.07.008

Saji VS (2020) Wax-based artificial superhydrophobic surfaces and coatings. Colloids Surf Physicochem Eng Asp 602:125132. https://doi.org/10.1016/j.colsurfa.2020.125132

Shen W, Zhang H, Ettl R (2005) Chemical composition of "AKD vapour" and its implication to AKD vapour sizing. Cellulose 12:641–652. https://doi.org/10.1007/s10570-005-9010-7

Soares S, Camino G, Levchik S (1995) Comparative study of the thermal decomposition of pure cellulose and pulp paper. Polym Degrad Stab 49:275–283

Sofla MRK, Brown RJ, Tsuzuki T, Rainey TJ (2016) A comparison of cellulose nanocrystals and cellulose nanofibres extracted from bagasse using acid and ball milling methods. Adv Nat Sci Nanosci Nanotechnol 7:035004. https://doi.org/10.1088/2043-6262/7/3/035004

Song C (2006) Global challenges and strategies for control, conversion and utilization of CO_2 for sustainable development involving energy, catalysis, adsorption and chemical processing. Catal Today 115:2–32. https://doi.org/10.1016/j.cattod.2006.02.029

Tulloch AP (1980) Beeswax—composition and analysis. Bee World 61:47–62. https://doi.org/10.1080/0005772X.1980.11097776

Wada M, Kondo T, Okano T (2003) Thermally induced crystal transformation from cellulose i-alpha to i-beta. Polym J 35:155–159

Wang Z, Li Y, Jiang L et al (2014) Relationship between secondary structure and surface hydrophobicity of soybean protein isolate subjected to heat treatment. J Chem 2014:1–10. https://doi.org/10.1155/2014/475389

Wang W, Lockwood K, Boyd LM et al (2016) Superhydrophobic coatings with edible materials. ACS Appl Mater Interfaces 8:18664–18668. https://doi.org/10.1021/acsami.6b06958

Wang Z, Ye Q, Liang X et al (2017) Paper-based membranes on silicone floaters for efficient and fast solar-driven interfacial evaporation under one sun. J Mater Chem A 5:16359–16368. https://doi.org/10.1039/C7TA03262E

Wang P, Qian X, Shen J (2018) Superhydrophobic coatings with edible biowaxes for reducing or eliminating liquid residues of foods and drinks in containers. BioResources 13:1–2

Willoughby BG (2016) The cole–cole plot for cure: the cure and reversion of natural rubber. J Appl Polym Sci. https://doi.org/10.1002/app.44085

Yuan Y, Li T, Zhang N et al (2016) Investigation on thermal properties of capric–palmitic–stearic acid/activated carbon composite phase change materials for high-temperature cooling application. J Therm Anal Calorim 124:881–888. https://doi.org/10.1007/s10973-015-5173-0

Zhang W, Lu P, Qian L, Xiao H (2014) Fabrication of superhydrophobic paper surface via wax mixture coating. Chem Eng J 250:431–436. https://doi.org/10.1016/j.cej.2014.04.050

Zhang X, Batchelor W, Shen W (2017) Building dual-scale roughness using inorganic pigments for fabrication of superhydrophobic paper. Ind Eng Chem Res 56:3618–3628. https://doi.org/10.1021/acs.iecr.7b00225